Materials Today: Proceedings xxx (xxxx) xxx

Contents lists available at ScienceDirect

Materials Today: Proceedings

journal homepage: www.elsevier.com/locate/matpr

Evaluation of mixed-mode stress intensity factor and T-stress in continuous epoxy glass functionally graded beam using digital image correlation

Ahmed M. Abood, Haider Khazal *, Abdulkareem F. Hasan

Mechanical Department, Engineering College, Basrah University, Iraq

ARTICLE INFO

Article history:
Received 3 March 2021
Accepted 9 March 2021
Available online xxxx

Keywords:
Continuous functionally graded materials
Digital image correlation
Epoxy/glass composite
Mixed-mode
T- stress

ABSTRACT

In the present study, the fracture parameters and crack tip deformation field in continuous functionally graded (FG) glass-filled epoxy composite were experimentally investigated employing digital image correlation. Beams with monotonic variation Young's modulus and cracks along the variation were studied. Two specimens with single edge cracks were examined in different crack positions in relation to the increase or decrease in Young's modulus. The mechanical properties of the FG composite were extracted by performing a tensile test of samples machined according to ASTM D638. The stress intensity factors and T- stresses (high order term) were evaluated from the displacement field by adopting William's series. This is the first research which calculated the mixed-mode stress intensity factors, as well as the T-stress in beam made of continuous epoxy glass functionally graded beam using DIC technique. The crack tip was elastically protected on the compliant side of the specimen unlike the crack on the stiffer side.

Selection and peer-review under responsibility of the scientific committee of the Emerging Trends in Materials Science, Technology and Engineering.

1. Introduction

The technological demand for new composite structures that are able to withstand in extreme conditions during operation without changing their characteristics is increasing. The concept of functionally graded materials (FGMs) was suggested in Japan in 1980. One of the main issues in the design of modern composites is to combine the conflicting thermo-mechanical properties into one component. Hence, sudden changes in their properties result in a reduction in the local stress concentration [1]. Because of their unique and efficient performance, FGMs are used in many applications (e.g. biomedical appliances, prosthetics, aviation transport, nuclear applications, energy, cutting tools, and sensors). [2] Fracture analysis of FGMs has been experimentally and numerically studied in different ways, but most of these studies focus on numerical rather than analytical approaches. Kim and Paulino [3] analysed the mixed-mode crack growth in FGMs by developing an automatic simulation of the propagation process in homogenous materials, using finite elements in combination with the remeshing algorithm. Rao and Rahman [4] presented the use of the Galerkin-based meshless method to investigate the fracture parameters in stationary cracks in FGMs and developed two interaction integral methods for mixed-mode analysis. Bayesteh and Mohammadi [5] used extended finite element method (XFEM) to evaluate stress intensity factors and study crack propagation in isotropic and orthotropic FGMs. The crack tip singularity was reduced by the enrichment of this region. Khazal et al. [6] developed an extended free Galerkin method for fracture analysis in isotropic and orthotropic FGMs and explained the calculation of the SIF by the interaction integral method. Garg and Pant [7] used a modified element free Galerkin method (EFGM) for thermoelastic fracture simulation of FGMs, to solve the heat transfer problem. Khazal and Salih [8] studied the mixed-mode and non-proportional load influence on crack propagation in FGMs by employing the extended free Galerkin method. Moreover, several researchers studied FGMs and related issues experimentally. Butcher et al. [9] prepared FGMs made from epoxy-glass composites for which the Young's modulus varied as a function of the position. Experimental estimation of the fracture parameters using coherent gradient sensing (CGS) for cracked FGMs and a homogeneous substance in a perpendicular pattern with an elastic modulus gradient. Rousseau et al. [10] achieved an experimental estimation of the fracture parameters using coherent gradient

* Corresponding author.
E-mail address: haiderkhazal@gmail.com (H. Khazal).

https://doi.org/10.1016/j.matpr.2021.03.233
2214-7853/
Selection and peer-review under responsibility of the scientific committee of the Emerging Trends in Materials Science, Technology and Engineering.

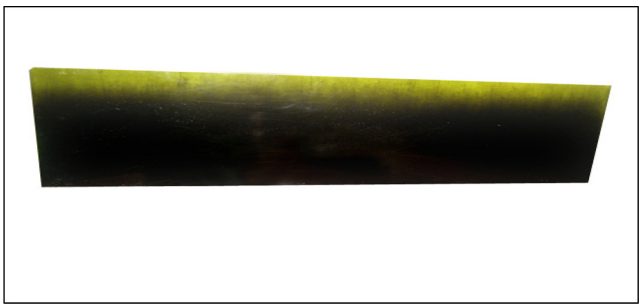

Fig. 1. Continuous FG epoxy-glass composite.

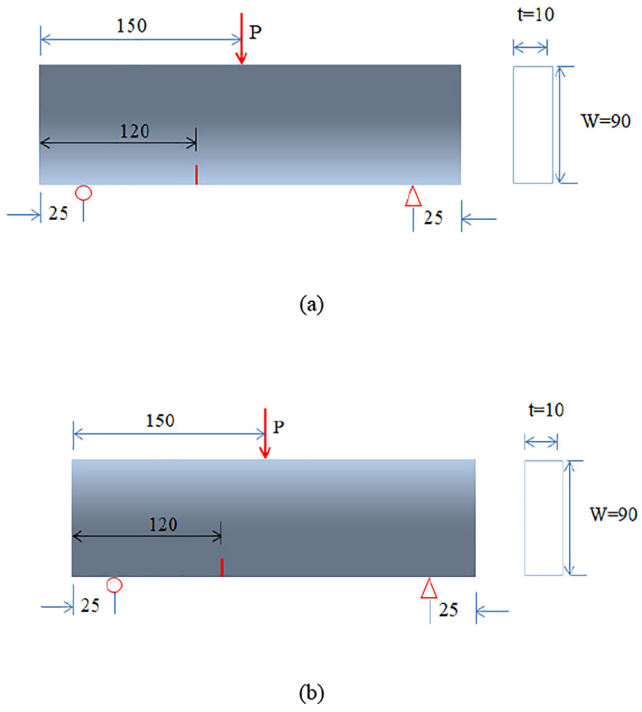

Fig. 2. FGM specimens with single edge crack on (a) compliant side, (b) stiff side.

Table1
Elasticity Moduli and Poisson's ratios corresponding to volume fractions.

Young's modulus (MPa)	Poisson's ratio	Volume fraction
1128	0.39	0.0
1130	0.34	0.027
1885	0.32	0.213
2230	0.31	0.261
2618	0.3	0.298

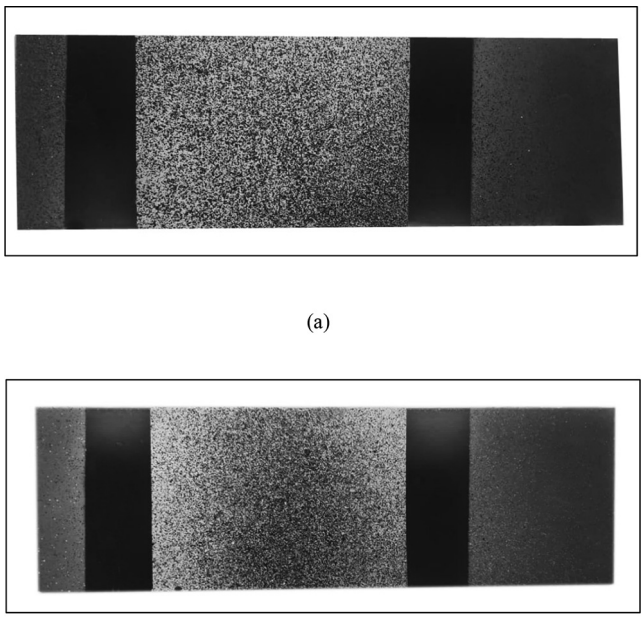

Fig. 3. Creating random patterns on the specimen surfaces (a) sample No.1, (b) sample No.2.

Fig. 4. Mixed-mode test of epoxy/glass FGM.

sensing (CGS) for cracked FGMs and a homogeneous substance in a perpendicular pattern with an elastic modulus gradient. Marur et al. [11] analysed the singularity around the crack tips in FGMs using FEM by considering different positions of cracks in the graded zone and calculating the SIFs and energy release rate. Rousseau et al. [12] studied the deformity of the crack tip in epoxy-glass composite under static and dynamic load by using High-speed photography coupled with (CGS) to investigate the immediate deformation in FG beam with linear Young's modulus variation. Kitey et al. [13] determined the influence of the reinforcement particle size and strength of interface adhesion in epoxy-glass composites. CGS and high photography used to evaluate the SIFs and the crack propagation velocity. Bueno and Lambros [14] studied the fracture behaviour in a polymer matrix FGM composite. They determined the SIFs and T-stress values using digital image correlation (DIC) to calculate the displacement field around the crack tip under mixed-mode loading conditions. Kirugulige and Tippur [15] prepared an FGM from an epoxy-glass composite with cracks along the direction of change in elastic properties in the FGM. A mixed-mode dynamic loading CGS technique was used to observe the

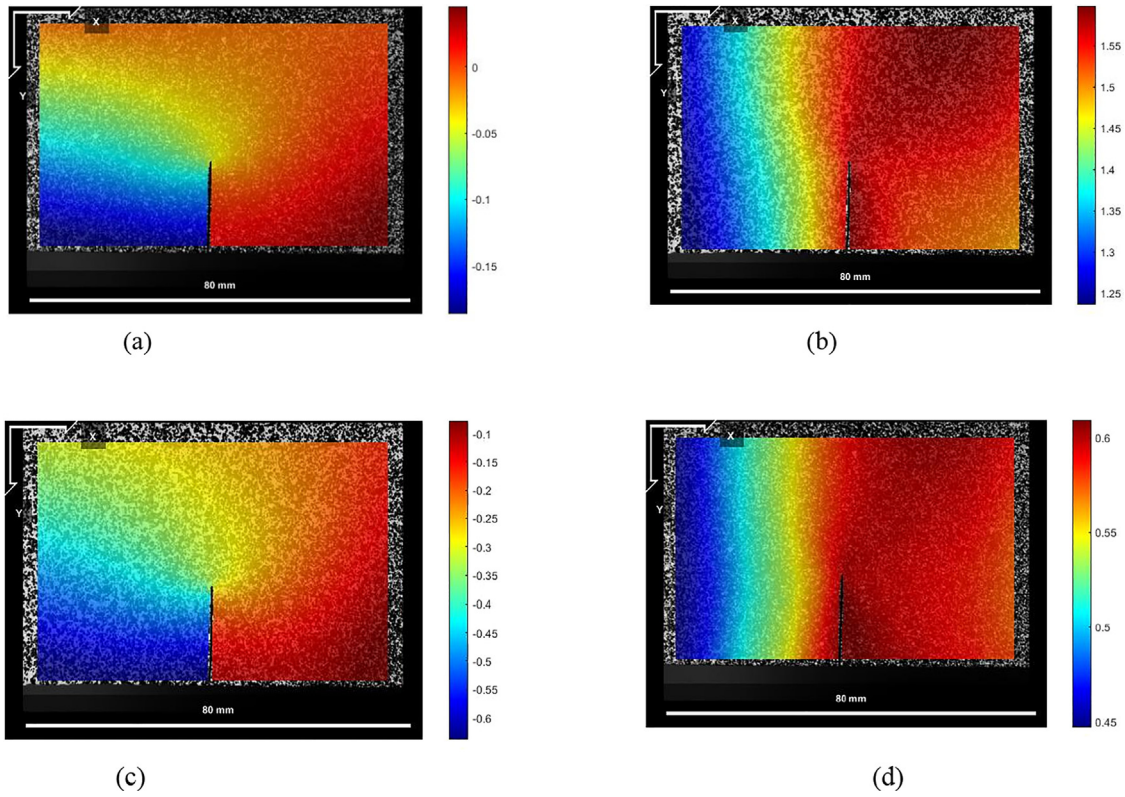

Fig. 5. Displacement field in X and Y direction, respectively (a), (b) for sample No.1 at F = 2540 N; (c), (d) for sample No.2 at F = 1128 N. Fig. 6 shows the horizontal (1)*U* and vertical (2)*U* displacements for sample No.1 and No.2 that were obtained by FE solution.

deformation in the crack tip after applying the load where the crack being started. Jin et al. [16] DIC was used to examine fracture parameters of a FGM specimen made of ZrO_2/NiCr. They investigated the effect of variation in the mechanical properties of ceramic/metal composite exposed to a quasi-static mixed-mode. Yates et al. [17] solved the fracture problem under periodic load by using DIC to determine the displacement full-field and then computing SIFs, T_ stress, and the crack tip open angle from these obtained data using William's series to solve the deformation field. They improved the technique for describing the displacement field at the crack tip based on the outcome of DIC. M.R. Yadegari et al. [18] considered different geometrical factors of V-notches, such as depth and angle of opening, to show the effect of these parameters on SIFs. A specimen made from polymethylmethacrylate (PMMA) with edge V-notch was tested using DIC under mode I. They found that the SIF values for 120° V-notches were greater than those for 30° V-notches. Abshirini et al. [19] studied the influence of crack length, depth and the distance between two notches by calculating the SIFs using DIC, neglecting the rigid body motion and rotation in the displacement field. The DIC results were obtained using the least square algorithm. They determined the SIFs for two parallel cracks in the PMMA plate exposed to tensile loading. Good results were obtained from both the experimental and numerical approaches. Farouq et al [20] experimentally investigated the step wise functionally graded epoxy/glass composite employing DIC measurements. An extended element free Galerkin method was adopted to prove the applicability of DIC methods in fracture analysis. Additionally, many studies have been dedicated to understand the influence of T-stress on the stability of the crack paths. Cotterell and Rice [21] determined the fracture parameters for a small kinked crack. The comparison between these results and those for a circular arc and a straight kinked crack showed that first-order solutions are more precise than solution for great drift. From straightness measurements, the crack path showed stability for negative T-stresses and instability for positive one. Ayatollahi et al. [22] developed an FEM for determining T-stress and found that the result was more trustworthy for mode I condition. They proposed a method to determine the T-stress for mixed-mode

Table 2
Experimental results of SIFs (MPa$\sqrt{m}$) and T-stress (MPa) at five different numbers of terms.

Load (N)	No. of terms	KI	KII	T-stress	Load (N)	No. of terms	KI	KII	T-stress
637	3	6.393	4.567	0.874	1913	3	32.509	7.029	1.482
	4	6.319	5.827	0.697		4	32.091	9.001	1.22
	5	6.386	5.979	0.445		5	32.413	9.27	0.774
	6	6.319	5.661	0.476		6	32.049	8.828	0.847
	7	6.181	6.039	0.308		7	31.484	9.425	0.583
1275	3	19.214	4.567	0.874	2540	3	49.73	11.404	1.806
	4	18.93	5.827	0.697		4	49.125	14.44	1.423
	5	19.144	5.979	0.445		5	49.601	14.823	0.781
	6	18.917	5.661	0.476		6	48.98	14.054	0.898
	7	18.547	6.039	0.308		7	48.155	14.898	0.521

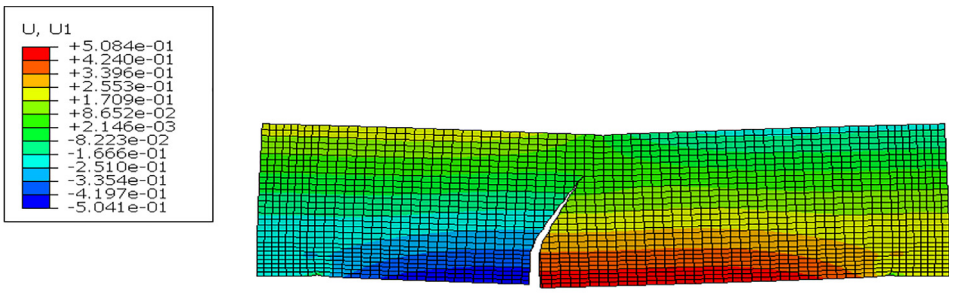

(a)

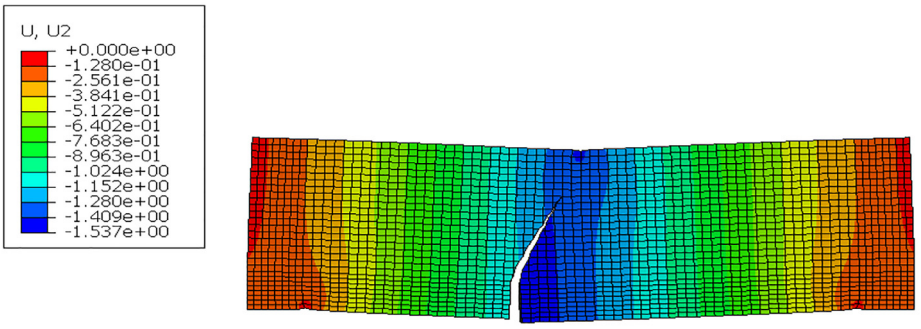

(b)

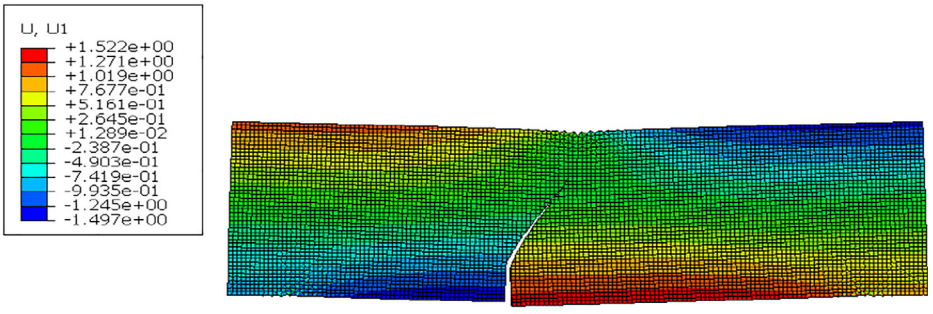

(c)

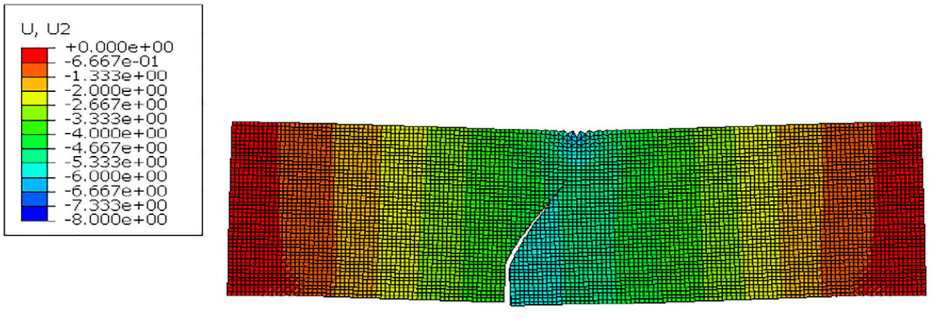

(d)

Fig. 6. Horizontal and vertical displacements (a), (b) for sample No.1 at 2540 N; (c), (d) for sample No.2 at 1128 N.

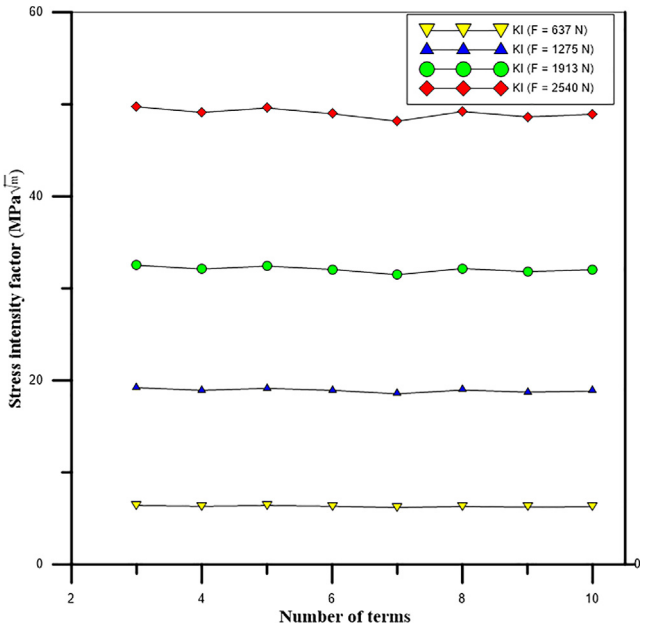

Fig. 7. Variation of SIF (KI) with number of terms.

conditions without the SIFs. It was pointed out that the T-stress values for shear were greater than those for tension. Smith et al. [23] employed the maximum tensile strength theory to study the fracture parameters for mixed-mode using PMMA material with a crack oriented towards a certain angle. They found that for the positive values of T-stress, there was a smaller scale yielding, and failure occurred when the non-singular term reached a critical value of brittle fracture. [24,25] used the numerical methods in finding T-stress in FGM. These articles demonstrate good computational accuracy.

This study investigates the manufacturing of continuous FGM made from epoxy resin and glass sphere. The mechanical properties and fracture parameters were experimentally calculated. DIC was used to capture the displacement field around the crack tip, and then William's series was employed to solve the deformation field to evaluate the SIFs and T-stresses. A single edge crack beam was examined under mechanical load in a mixed-mode condition. Two crack configurations were considered: in the first one, the crack was placed on the compliant (epoxy-rich side) and the second one had a crack on the stiff (glass-rich) side. The experimental results then verified numerically using ABAQUS program, and good agreement was obtained.

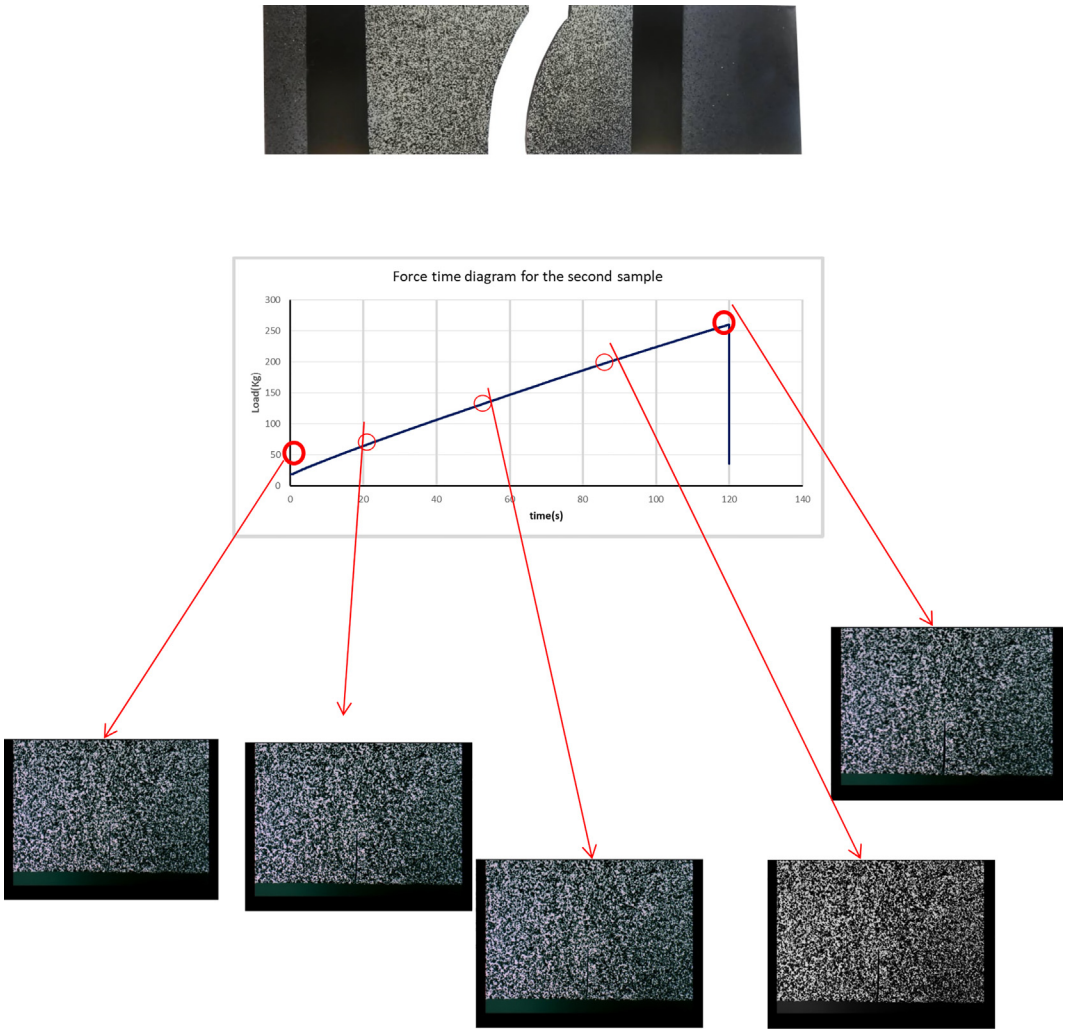

Fig. 8. Load-time diagram for specimen No.1.

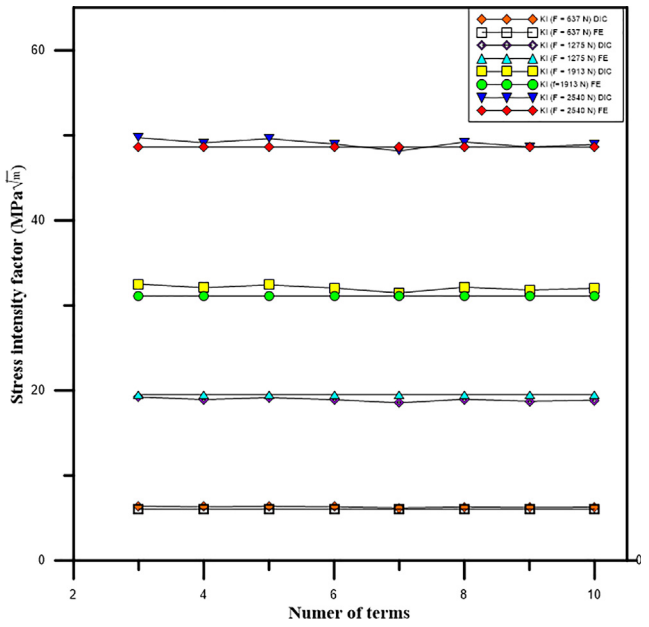

Fig. 9. Comparison of SIF (KI) results obtained from DIC and FE methods at different number of terms and load range 637.65–2540.79 N for sample No.1.

Table 3
Relative error between DIC and FE results at loads 637.65–2540.79 N for sample No.1.

Load (N)	KI (FE) (MPa$\sqrt{m}$)	KI (DIC) (MPa$\sqrt{m}$)	Relative error %	T-stress (FE) (MPa)	T-stress (DIC) (MPa)	Relative error %
637.65	6.009	6.319	4.9	0.249	0.275	−9.4
1275.3	19.516	18.93	3	0.761	0.697	9.1
1913	31.105	32.091	3	1.314	1.22	−7.7
2540.79	48.609	49.125	1	1.517	1.423	6.6

2. Experiment

2.1. Preparation of functionally graded material

A continuous FGM was manufactured by the hand lay-up method. The epoxy/glass composite was prepared by mixing the components in adequate proportions, using a 30% volume fraction of 90 μm mean diameter glass particles to produce spatial variation in elastic properties. Low-viscosity epoxy resin (ρ = 1050 kg/m^3) was used as a matrix. An acrylic mould with dimensions 300×90×10 mm was prepared using a laser computer numerically controlled machine, holding it in vertical position so that the side with 90 mm length was the vertical dimension, having 300 mm length and 10 mm in thickness as shown in Fig. 1. Two specimens were prepared to be examined as three-point bending beams with a single edge crack as shown in Fig. 2.

2.2. Mechanical properties of epoxy/glass composite

The elastic properties of the manufactured functionally graded epoxy glass composite were extracted according to ASTM D638. Standard tensile test samples were machined from the functionally graded beam using a milling machine to specify the standard sample type 1. The thickness of the specimen was 7 mm, its overall length was165 mm, gauge length was 57 mm, width of its narrow side was 13 mm, and fillet radius was 76 mm. The percentage of glass in a FG beam was calculated using Image J program. A portion of the created beam was cut to a certain length, and then parts were cut with a precision of 1.5×1*cm*. Young's moduli and Poisson's ratio corresponding to the different volume fraction are shown in. Table1.

As illustrated in Table 1, Young's modulus increased while Poisson's ratio decreased as the volume fraction of the filler particles increased.

3. Digital image correlation method

3.1. Specimen preparation and experimental set up

Two specimens of FGMs were prepared to be examined as three-point bending beam in a mixed-mode condition. A single edge crack was made by inserting a fresh razor blade into the specimen. In the first specimen (No.1), the crack was placed on the compliant side (epoxy-rich side), while in the second specimen (No.2), it was placed on the stiff side (glass-rich side), a random pattern of speckles was created on the specimen surface by applying white colour and then spraying it with black colour, as shown in Fig. 3.

The light intensity can be measured by discretion of the intensity of the particular area into the range known as the grey scale for each pixel, then by use of computer software the small area in the reference and deformed image are traced. The set of different pixels and grey scales is called subset. The reference and deformed images were compared each subset to determine their correlation coefficient [18].

A GOTCH machine was used in the test at grip speed (1 mm/min). An ART CAM −320p CCD camera with a Fujian lens with 2288×1700 pixels resolution was used to image the experiment as depicted in Fig. 4. White lights were used to illuminate the surface of the specimen. Each sample was examined at different loads.

Table 4
Experimental results of SIF (MPa$\sqrt{m}$) and T-stress (MPa) at five different numbers of terms.

Load (N)	No. of terms	KI	KII	T-stress	Load (N)	No. of terms	KI	KII	T-stress
284	3	6.483	2.252	0.511	843	3	21.74	5.052	0.973
	4	6.566	2.83	0.499		4	22.05	6.287	0.96
	5	6.599	2.934	0.369		5	22.122	6.495	0.702
	6	6.522	2.789	0.361		6	21.933	6.146	0.681
	7	6.475	2.662	0.401		7	21.761	5.954	0.738
569	3	13.998	5.052	0.973	1128	3	29.328	8.467	1.501
	4	14.19	6.287	0.96		4	29.683	10.812	1.474
	5	14.275	6.495	0.702		5	29.763	11.198	1.011
	6	14.1006	6.146	0.681		6	29.49	10.513	0.956
	7	14.001	5.954	0.738		7	29.101	10.382	0.993

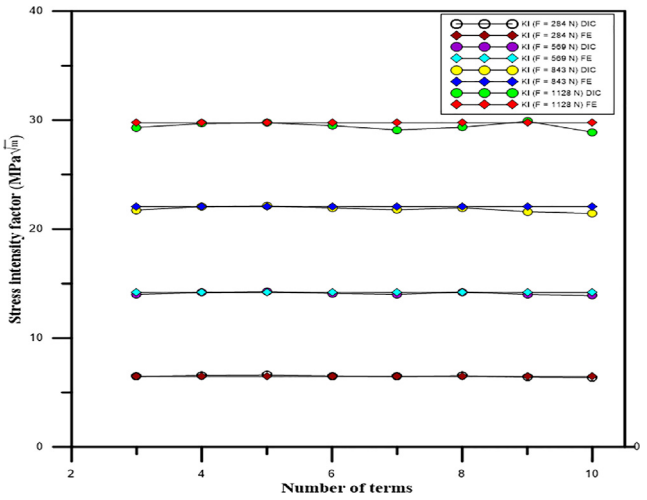

Fig. 10. Comparison between experimental and numerical results for sample No.2 at load range 284.5–1128.15 N for sample No.2.

Table 5
Relative error between DIC and FE results at load range 284.5–1128.15 N for sample No.2.

Load (N)	KI (FE)	KI (DIC)	Relative error %	T-stress (FE)	T-stress (DIC)	Relative error %
284.5	6473	6.566	−1.4	0.575	0.511	12.5
569	14.638	14.19	3.1	0.678	0.702	3.4
843.66	22.536	22.05	2.2	1.707	1.618	5.5
1128.15	30.115	29.763	1.1	1.341	1.474	9

3.2. Calculation of stress intensity factors and T-stress

The fracture parameters in this study were estimated by employing William's series. After the deformation field of speckles was captured by digital image measurement, this field was used to evaluate the SIFs and T-stress in the crack tip region. First, the crack tip location, where the estimated values of the SIFs depend on the crack tip coordinates set in the algorithm, must be known. The infinite series that represents the displacement field can be written as [16]

$$\text{Model}\begin{Bmatrix} u_1 = \sum_{n=1}^{\infty} \frac{r_2^{\frac{n}{2}}}{2\mu} a_n \left\{ \left[\kappa + \frac{n}{2} + (-1)^n\right] cos\frac{n\theta}{2} - \frac{n}{2} cos\frac{(n-4)\theta}{2} \right\} \\ v_1 = \sum_{n=1}^{\infty} \frac{r_2^{\frac{n}{2}}}{2\mu} a_n \left\{ \left[\kappa - \frac{n}{2} - (-1)^n\right] sin\frac{n\theta}{2} + \frac{n}{2} sin\frac{(n-4)\theta}{2} \right\} \end{Bmatrix} \quad (1)$$

$$\text{ModelII}\begin{Bmatrix} u_{II} = -\sum_{n=1}^{\infty} b_n \left\{ \left[\kappa + \frac{n}{2} - (-1)^n\right] sin\frac{n\theta}{2} - \frac{n}{2} sin\frac{(n-4)\theta}{2} \right\} \\ v_{II} = \sum_{n=1}^{\infty} b_n \left\{ \left[\kappa - \frac{n}{2} + (-1)^n\right] cos\frac{n\theta}{2} + \frac{n}{2} cos\frac{(n-4)\theta}{2} \right\} \end{Bmatrix} \quad (2)$$

Where, u and $v$are the displacement components in X and Y direction, respectively, $\mu$is the rigidity modulus, κ = (3−ν)/ (1 + ν) for plane stress, κ = (3−4ν) for plane strain. In addition, $a$and b are constants to be determined, while the first terms of parameters a_1, b_1 refer to mode I and mode II SIFs, respectively. When n = 2, T-stress can also be determined, (r, ɵ) being the polar coordinates of the crack tip. The mixed-mode field obtained from the DIC method can be extracted by superimposing the displacement fields of modes I and II. The displacement field in Eqs. (1 and 2) can be expressed as

$$\frac{r_m^{\frac{n}{2}}}{2\mu}\left\{\left[\kappa + \frac{n}{2} + (-1)^n\right] cos\frac{n\theta_m}{2} - \frac{n}{2} cos\frac{(n-4)\theta_m}{2}\right\} \quad (3)$$

$$\frac{-r_m^{\frac{n}{2}}}{2\mu}\left\{\left[\kappa + \frac{n}{2} - (-1)^n\right] sin\frac{n\theta_m}{2} - \frac{n}{2} sin\frac{(n-4)\theta_m}{2}\right\} \quad (4)$$

$$\frac{r_m^{\frac{n}{2}}}{2\mu}\left\{\left[\kappa - \frac{n}{2} - (-1)^n\right] sin\frac{n\theta_m}{2} + \frac{n}{2} sin\frac{(n-4)\theta_m}{2}\right\} \quad (5)$$

$$\frac{r_m^{\frac{n}{2}}}{2\mu}\left\{\left[\kappa - \frac{n}{2} + (-1)^n\right] cos\frac{n\theta_m}{2} + \frac{n}{2} cos\frac{(n-4)\theta_m}{2}\right\} \quad (6)$$

$$\begin{Bmatrix} u_1 \\ . \\ . \\ . \\ u_m \\ v_1 \\ . \\ . \\ . \\ v_m \end{Bmatrix} \begin{bmatrix} f_{1,1}\cdots f_{n,1} g_{1,1}\cdots g_{n,1} \\ . \\ . \\ . \\ f_{1,m}\cdots f_{n,m} g_{1,m}\cdots g_{n,m} \\ h_{1,1}\ldots h_{n,1} l_{1,1}\ldots l_{n,1} \\ . \\ . \\ . \\ h_{1,m}\ldots h_{n,m} l_{1,m}\ldots l_{n,m} \end{bmatrix} \begin{Bmatrix} a_1 \\ . \\ . \\ . \\ a_n \\ b_1 \\ . \\ . \\ . \\ b_n \end{Bmatrix} \quad (7)$$

where $m$is the index of the data point, and $f_{n,m}$, $g_{n,m}$, $h_{n,m}$, $l_{n,m}$ are knowing function of (r, ɵ). By expanding Eqs. (1 and 2), cancelling the terms of order $r^{\frac{3}{2}}$ and above, and applying the T-stress and SIFs as depicted in the equations below.

$$u = \frac{KI}{2\mu}\sqrt{\frac{r}{2\pi}}\cos\frac{\theta}{2}\left(\kappa - 1 + 2\sin^2\frac{\theta}{2}\right) + \frac{KII}{2\mu} \times \sqrt{\frac{r}{2\pi}}\sin\frac{\theta}{2}\left(\kappa + 1 + 2\cos^2\frac{\theta}{2}\right) + \frac{T}{8\mu} r(\kappa+1)\cos\theta \quad (8)$$

$$v = \frac{KI}{2\mu}\sqrt{\frac{r}{2\pi}}\sin\frac{\theta}{2}\left(\kappa + 1 - 2\cos^2\frac{\theta}{2}\right) - \frac{KII}{2\mu}\sqrt{\frac{r}{2\pi}}\cos \times \frac{\theta}{2}\left(\kappa - 1 - 2\cos^2\frac{\theta}{2}\right) + \frac{T}{8\mu} r(\kappa-3)\sin\theta \quad (9)$$

it can be illustrated that:

$$\text{KI} = a_1\sqrt{2\pi}, \text{KII} = -b_1\sqrt{2\pi}, \text{T} = 4\text{a}2 \quad (10)$$

K_I and K_{II} are the SIFs for mode I and mode II, respectively, and T is the T-stress.

In Eq. (7), no term for rigid body motion is included; hence, by adding constants to this equation rigid body motion and translation, rigid body and translation can be compensated.

$$\begin{Bmatrix} u_1 \\ . \\ . \\ . \\ u_m \\ v_m \\ . \\ . \\ . \\ v_m \end{Bmatrix} \begin{bmatrix} 1 f_{1,1..} f_{n,1} 0 g_{1,1}\cdots g_{n,1} - r\sin\theta_1 \\ .. \\ .. \\ .. \\ 1 f_{1,m}\cdots f_{n,m} 0 g_{1,m}\cdots g_{n,m} - r\sin\theta_m \\ 0 h_{1,1}\ldots h_{n,1} 1 l_{1,1}\ldots l_{n,1} r_1 \sin\theta_1 \\ .. \\ .. \\ .. \\ 0 h_{1,m}\ldots h_{n,m} 1 l_{1,m}\ldots l_{n,m} r_m \cos\theta_m \end{bmatrix} \begin{Bmatrix} a_0 \\ a_1 \\ . \\ . \\ . \\ a_n \\ b_0 \\ b_1 \\ . \\ . \\ . \\ b_n \\ R \end{Bmatrix} \quad (11)$$

where, a_0, b_0 and R are the compensation terms for the translation and rotation of the rigid body.

4. Results and discussion

The DIC method was used to calculate the SIFs for the crack tip of the epoxy/glass FGM. The reference image was captured according to the aforementioned procedure. The deformed image was then recorded. By considering the area around the crack tip and the number of terms used in William's equations, the displacement field was applied to MATLAB code to estimate the SIFs and T- stresses of the FGM specimens

Horizontal and vertical (u, v) displacement contours of the FG beam from the DIC test at different loads are clarify in Fig. 5.

Experimental results of SIFs and T-stress for specimen with crack on the compliant side for load range 637–1912 N are illustrated in Table 2.

As appear in Fig. 7. The system was found converge and was well balanced when using a coefficient from eight terms in William's equations.

The load time diagram for sample No.1 Fig. 8 shows that the critical load is approximately 2540 N and the time spent to reach this load is 119 s. Meanwhile, from the load time diagram for sample No.2, it can be seen that the crack starts to propagate at 1128 N, and the time required to reach the critical load is 58.5 s. The experimental results were verified using the ABAQUSE FE application. The material properties were defined as a function of one independent variable, which was temperature in this case. Young's modulus and Poisson's ratio were specified at different temperatures. The value of the independent variable had to be increased in a way similar to the variation in the elastic properties. Linear interpolation was then performed between these values. This study used the analytical field in the Y direction to express the temperature distribution. Fig. 9 illustrates the comparison between DIC and numerical results for FGM sample No.2. Table 3 shows the relative error for the load range 637–1912 N.

For sample No.2, where the crack was placed on the stiff side, the experimental results for the SIFs and T-stresses at loads 284.5–1128 N are shown in Table 4. Fig. 10 appears the comparison between the experimental and the numerical results for this sample at different loads. Table 5 illustrates the relative error between the experimental and numerical results for sample No.1. Good agreement was captured between the experimental and numerical results of SIFs (KI) and T-stresses, while the results of KII showed disagreement due to dependence on coefficient with high order terms in William's equations [17,26]. It is worth noting that the size of the data collection that was adopted in the DIC calculations was 24 mm, as the verifications found stability of results with this variable starting from 20 mm.

5. Conclusion

In this study, an epoxy /glass FGM was manufactured using the hand lay-up method. Mechanical properties were extracted by tensile testing according to ASTM D638 to determine the elastic modulus, it which was changed continuously as a function of the position. SIFs and the non-singular term of T-stresses were evaluated experimentally by employing DIC, and the experimental results were verified using the ABAQUS FE program. The results of this study can be summarized in the following points:

When the crack was placed on the compliant side, the crack growth was delayed and the time required for failure increased, compared to when the crack was placed on the stiff side.

The specimen with crack tip location on the stiff side experienced higher SIFs than the one with cracks on the compliant side.

Good agreement was found between the experimental and numerical results for SIFs KI and high-order terms of T-stresses. The results of KII show disagreement due to the dependence on coefficient with high order term in William's equation.

CRediT authorship contribution statement

Ahmed M. Abood: Conceptualization, Methodology, Software, Data curation. **Haider Khazal:** Writing - original draft, Visualization. **Abdulkareem F. Hasan:** Investigation, Supervision, Software, Validation, Writing - review & editing.

Declaration of Competing Interest

The authors declare that they have no known competing financial interests or personal relationships that could have appeared to influence the work reported in this paper.

Acknowledgements

The authors are grateful to the IBEM laboratory of the University of Tehran for its assistance in DIC tests.

References

[1] G. Udupa, S.S. Rao, K.V. Gangadharan, Functionally graded composite: an overview, Procedia Matear. Sci. 5 (2014) 1291–1299.
[2] Y. Miyamoto, W.A. Kaysser, B.H. Rabin, A. Kawasaki, Renee G. Ford. Functionally graded materials Design, Processing and Applications. Springer Science+ Business Media. ISBN 978-0-412-60760-8. 1999.
[3] J.H. kim, G.H. Paulino. Consistent Formulations of the Interaction Integral Method for Fracture of Functionally Graded Materials. Journal of Applied Mechanics. 72. 351-364. 2005.
[4] B.N. Rao, S. Rahman, Mesh-free analysis of cracks in isotropic functionally graded materials, Eng. Fract. Mech. 70 (1) (2003) 1–27.
[5] H. Bayesteh, S. Mohammadi, XFEM fracture analysis of orthotropic functionally graded materials, Compos. B Eng. 44 (1) (2013) 8–25.
[6] H. Khazal, H. Bayesteh, S. Mohammadi, S.S. Ghorashi, A. Ahmed, An extended element free Galerkin method for fracture analysis of functionally graded materials, Mech. Adv. Mater. Struct. 23 (5) (2016) 513–528.
[7] S. Garg, M. Pant, Numerical simulation of adiabatic and isothermal cracks in functionally graded materials using optimized element-free Galerkin method, J. Therm. Stresses 40 (7) (2017) 846–865.
[8] H. Khazal, N.A. Saleh, XEFGM for crack propagation analysis of functionally graded materials under mixed-mode and non-proportional loading, Mech. Adv. Mater. Struct. 26 (11) (2019) 975–983.
[9] R.J. Butcher, C.-E. Rousseau, H.V. Tippur, A functionally graded particulate composite: preparation, measurements and failure analysis, Acta. Mater. 47 (1) (1998) 259–268.
[10] C.-E. Rousseau, H.V. Tippur, compositionally graded material with cracks normal to the elastic gradient, Acta. Mater. 28 (2000) 4021–4033.
[11] P.R. Marur, H.V. Tippur, Numerical analysis of crack-tip fields in functionally graded materials with a crack normal to the elastic gradient, Int. J. Solids Struct. 37 (2000) 5353–5370.
[12] C.-E. Rousseau, H.V. Tippur, Evaluation of crack tip fields and stress intensity factors in functionally graded elastic materials: Cracks parallel to elastic gradient, Int. J. Fract. 114 (2002) 87–111.
[13] R. Kitey, H.V. Tippur, Role of particle size and filler–matrix adhesion on dynamic fracture of glass-filled epoxy. I. Macromeasurements, Acta. Mater. 53 (2005) 1153–1165.
[14] J. Abanto-Bueno, J. Lambros, An Experimental Study of Mixed Mode Crack Initiation and Growth in Functionally Graded Materials, Exp. Mech. 46 (2) (2006) 179–196.
[15] M.S. Kirugulige, H.V. Tippur, Mixed-Mode Dynamic Crack Growth in Functionally Graded Glass-Filled Epoxy, Exp. Mech. 46 (2) (2006) 269–281.
[16] X. Jin, L. Wu, L. Guo, H. Yu, Y. Sun, Experimental investigation of the mixed-mode crack propagation in ZrO2/NiCr functionally graded materials, Eng. Fract. Mech. 76 (2009) 1800–1810.
[17] J.R. Yates, M. Zanganeh, Y.H. Tai, Quantifying crack tip displacement fields with DIC, Eng. Fract. Mech. 77 (2010) 2063–2076.
[18] B. Al Hayan, H. Ilhan,, Image transmission over decode and forward based cooperative wireless multimedia sensor networks for Rayleigh fading channels in medical Internet of Things (MIoT) for remote health-care and health communication monitoring,, J. Med. Imaging Heal. Informatics 10 (1) (2020) 160–168, https://doi.org/https://doi.org/10.1166/jmihi.2020.2691.
[19] M. Abshirini, M.Y. Dehnavi, M.A. Beni, N. Soltani, Interaction of two parallel U-notches with tip cracks in PMMA plates under tension using digital image correlation, Theor. Appl. Fract. Mech. 70 (2014) 75–82.

[20] W. Farouq, H. Khazal, A.K.F. Hassan, Fracture analysis of functionally graded material using digital image correlation technique and extended element-free Galerkin method, Opt. Lasers Eng. 121 (2019) 307–322.
[21] B. Cotterell, J.R. Rice, Slightly curved or kinked cracks, Int. J. Fract. 16 (2) (1980) 155–169.
[22] M.R. Ayatollahi, M.J. Pavier, D.J. Smith, Determination of *T* -stress from finite element analysis for mode I and mixed mode I/II loading, Int. J. Fract. 19 (1998) 283–298.
[23] D.J. Smith, M.R. Ayatollahi, M.J. Pavier, On the consequences of T-stress in elastic brittle Fracture, Proc. Royal Soc. 462 (2006) 2415–2437.
[24] B. Al Hayani, H. Ilhan, Visual sensor intelligent module based image transmission in industrial manufacturing for monitoring and manipulation problems, J Intell Manuf 32 (2021) 597–610, https://doi.org/10.1007/s10845-020-01590-1.
[25] A. Memari, Coupled numerical analysis for in-plane elastic T-stress evaluation in isotropic FG solids, Eng. Anal. Boundary Elem. 120 (2020) 1–12.
[26] H. Khazal, A.K.F. Hassan, W. Farouq, H. Bayesteh, Computation of fracture parameters in stepwise functionally graded materials usin digital image correlation technique, Mater. Perform. Charact. 8 (1) (2019) 344–354.